Nanoscale

PAPER

View Article Online
View Journal | View Issue

Cite this: *Nanoscale*, 2019, **11**, 21856

DNA-based digital comparator systems constructed by multifunctional nanoswitches†

Hongmei Geng,[a,b] Chunyang Zhou*[a] and Chunlei Guo*[a,c]

Received 24th September 2019,
Accepted 24th October 2019

DOI: 10.1039/c9nr08216f

rsc.li/nanoscale

In this paper, we propose a strategy involving coupling DNA structural nanoswitches with toehold mediated strand displacement for constructing novel DNA-based digital comparator (DC) logic systems, which are a basic part of traditional electronic computers and can compare whether two or more input numbers are equal. However, when the number of DC inputs is increased to a certain level, the speed and quality of the computing circuit can be affected because of the limitations of conventional electronic computers when it comes to handling large-scale quantities of data. To solve this problem, in this work, we introduce a multi-input to multi-output DNA switch-based platform that can enable complex DC logical comparison. These multifunctional DNA-based switches, each including two hairpin-shaped molecular beacons and a G4/NMM complex, were used as platforms for the step-by-step realization of 2-3 DC, 3-3 DC, and 4-3 DC logic operations. Also, experiments were designed to further verify the excellent selectivity, achieving single-base mismatch operations with the digital comparator. Based on our design, comparators (">", "<" and "=") can be realized. Our prototype can inspire new designs and have intelligent digital comparator and in-field applications.

1. Introduction

Modern electronic microprocessors usually use semiconductor logic gates assembled on a silicon chip to enable efficient inter-gate communication.[1] Logic gates are devices that can recognize one or more input signals and process them through a certain input–output signal correlation pattern, producing a single binary output signal that can be defined as either low or high: a digital 0 or 1, respectively.[2] In electronic computing, higher-ordered logic circuits implement information processing and other complex functions at varying degrees of complexity through the wiring together of multiple requisite electronic logic devices, which is a significant challenge on a molecular scale.[3] Also, upon increasing the number of input signals to a certain level, a greater number of transistors and more complicated circuit connections will be needed, dramatically increasing the design complexity and manufacturing cost of electronic circuits. Other than that, the processing speed and quality of the circuits will be affected because the abilities of electronic computers to process such large amounts of data are limited. To solve these problems, logic operations based on DNA reactions come into play. Thanks to its amazing parallel computation abilities, predictable configuration and programmable sequences, DNA has been conceived as one of the most promising "intelligent nanomaterials", owing to the well-established base-pairings of A-T and G-C allowing the construction of DNA-based logic circuits.[4–17] To date, various well-designed DNA logic circuits have been realized to implement versatile functions, from data to information processing, based on different strategies, including DNA hybridization,[18–22] the use of functional DNA structures[23,24] and enzyme-catalyzed reactions.[25,26] In 2006, Winfree and coworkers first reported the design and experimental implementation of DNA logic circuits based on DNA hybridization, with functionality including AND, OR, and NOT gates, signal restoration, amplification, feedback, and cascading.[27] Tan and coworkers have constructed 3D DNA nanostructures as logic nanomachines to target overexpressed cancer cell biomarkers with bispecific recognition.[28] Zhang and coworkers have utilized DNAzymes and DNA catalysts to construct a series of logic gates, including YES, OR, and AND gates. In addition, a two-layer cascading circuit and a feedback self-catalysis circuit were also established in their work.[29] However, these logic operations based on the different reaction strategies mentioned above are all designed to implement a

[a]*The Guo China-US Photonics Laboratory, State Key Laboratory for Applied Optics, Changchun Institute of Optics, Fine Mechanics and Physics, Chinese Academy of Sciences, Changchun, Jilin, 130033, P. R. China. E-mail: guo@optics.rochester.edu, cyzhou@ciomp.ac.cn*
[b]*University of Chinese Academy of Sciences, Beijing 100049, China*
[c]*The Institute of Optics, University of Rochester, Rochester, New York, 14627, USA*
†Electronic supplementary information (ESI) available. See DOI: 10.1039/c9nr08216f

variety of basic or advanced logic functions; very few works have implemented logic computing systems based on specific functions that are expected to allow the realization of large-scale digital signal input.

In the last few decades, DNA has gained increasing recognition as a versatile and powerful building block for the fabrication of self-assembly nanostructures,[30] including the generation of hairpin structures *via* self-complementarity, guanosine (G)-rich sequences self-assembling in the presence of K^+ or NH^{4+} ions into G-quadruplex nanostructures, and cytosine (C)-rich strands assembling under appropriate pH conditions into i-motif structures that can be adapted as DNA switches.[31] The DNA switches are "responsive" DNA structures that can undergo structural or physical property changes in the presence of specific external stimuli. A number of DNA switches, such as aptamers, DNAzymes, molecular beacons and G-quadruplexes, have been shown to respond to a variety of stimuli, including proteins, ions and oligonucleotides.[32–37] In this work, through utilizing different designed DNA strands that use stimuli as input signals, some DNA switches have been adapted to a reaction platform to realize a DNA-based digital comparator system for the first time.

A molecular beacon (MB), or stem-loop folded hairpin deoxyribonucleic acid probe with a fluorophore and a quencher in close proximity at the two ends of the probe, shows decreased fluorescence emission due to fluorescence resonance energy transfer (FRET) between the labels at the two ends.[37] When binding to its complementary sequence or target, the stem-loop structure will be disrupted and induce increasing fluorescence related to the separation distance between the dual labels. As a kind of signal transducer, MBs present many advantages over quantum dots and nanoclusters, as MBs can not only shorten the reaction time through avoiding nanomaterial interactions capable of quenching fluorescence, but they are also easier to introduce into a DNA logic system *via* a toehold-mediated DNA strand displacement strategy. G-quadruplexes (G4s), which are guanine-rich DNA sequences that involve the enthalpically favorable reorganization of guanines to form planar structures through hydrogen bonding,[38] can generate a significantly enhanced fluorescence response when binding with some fluorescent dyes, such as *N*-methylmesoporphyrin IX (NMM) and protoporphyrin IX (PPIX). These intrinsic properties make MBs and G4s great DNA switch candidates with promising applications in the development of logic biocomputing.

Here, through the rational design of a series of nanoswitches using DNA structures including MBs and G4s as the reaction platform, which are allosterically controlled using specific DNA inputs with the corresponding fluorescence signals output in a controlled fashion, we have successfully realized a DNA-based digital comparator (DC) logic system. The DC logic operation is a basic unit in traditional electronic computers that can compare input numbers to see if they are equal. As shown in Fig. 1, the multifunctional DNA switch-based platform that we designed could also perform the function of comparing the input binary numbers shown in the equivalent traditional circuit diagrams. However, in traditional logic circuits, upon increasing the input binary numbers to a certain level, it is difficult to fulfill the DC function and

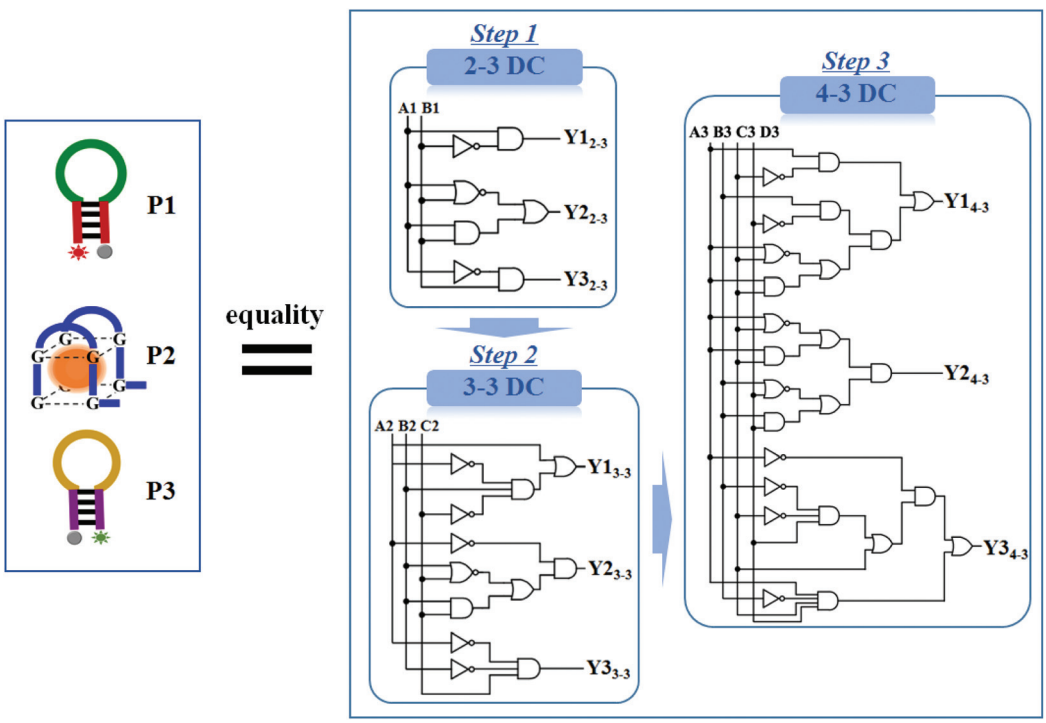

Fig. 1 A comparative description of digital comparators based on different reaction mechanisms, including a DNA-based platform and traditional electronic circuits.

achieve large-scale integration, since this greatly increases the design complexity and manufacturing cost of the integrated circuit.[39] To solve this problem, in this work, the DNA-based switches were integrated as a multifunctional platform for the step-by-step realization of 2-3 DC, 3-3 DC and 4-3 DC logic operations. What is important is that such a DNA-based DC system is expected to be able solve big data problems through hybridization reactions based on the Watson–Crick base-pairing principle, avoiding the issues of integrated circuit design complexity and manufacturing costs that are present in traditional computing.

Aside from the construction of a DNA-based DC system, the realization of DNA logic gates is of scientific interest for intelligent biosensing and diagnosis.[40–42] Sensitivity and specificity are significant in biosensing and can be realized through a multiple cascade strategy.[43] With two disease-related genes as inputs, in this work, the 2-3 DC was demonstrated for the first time to act as an intelligent biosensor to realize digital comparator functionality and achieve selectivity in gene detection with three output responses under logic circuit control.

2. Experimental section

2.1. Materials and apparatus

In this work, all DNA strands (HPLC) were bought from Sangon Biotechnology Company (Shanghai, China), and the DNA sequences are listed in the ESI (Table S1†). Acrylamide, tris(hydroxymethyl)aminomethane, ammonium persulfate, boric acid, and *N*,*N*′-methylenebisacrylamide were purchased from Aladdin Biochemical Technology Co. Ltd. EDTA was purchased from Sangon Biotechnology Company. *N*-Methyl mesoporphyrin IX was purchased from J&K Scientific Ltd. All chemicals were analytical reagents and used without further purification. The concentrations of the DNA sequences were quantified using NanoDrop One from Thermo with the following extinction coefficients ($\varepsilon_{260\ nm}$, $M^{-1}\ cm^{-1}$): A = 15 400; T = 8700; G = 11 500; and C = 7400. All solutions were prepared using ultrapure water (18.2 MΩ cm) obtained from a Milli-Q purification system.

The fluorescence emission spectra were collected using a Cary Eclipse fluorescence spectrophotometer purchased from Agilent Technologies in Tris-HCl buffer (20 mM Tris-HCl, 10 mM $MgCl_2$, 200 mM KCl, pH 8.0) at room temperature (Fig. S2†). The excitations of FAM, NMM, and Cy5 were performed at 494, 399, and 632 nm, respectively. The emissions of FAM, NMM, and Cy5 were recorded at 517, 609 and 663 nm. Native polyacrylamide gel electrophoresis experiments were conducted with an electrophoresis tank from Bio Rad. The gel images were obtained using a BioDoc-It2 imager from UVP.

2.2. Statistical analysis

Before the implementation of all the logic circuits, including 2-3 DC, 3-3 DC and 4-3 DC, optimization experiments were done during the hybridization of the DNA strands. First of all, for the 2-3 DC logic operation, the concentrations of the DNA switches $P1_{2\text{-}3}$, $P2_{2\text{-}3}$ and $P3_{2\text{-}3}$ were confirmed as 100 nM, 100 nM and 100 nM, respectively. The optimized concentrations of the inputs (A1 and B1) for the 2-3 digital comparator system were determined, based on the fluorescence intensities of FAM and Cy5, as 350 nM and 350 nM, respectively (Fig. S3†). Secondly, in the 3-3 DC logic operation, the concentrations of the DNA switches $P1_{3\text{-}3}$, $P2_{3\text{-}3}$ and $P3_{3\text{-}3}$ were confirmed as 100 nM, 100 nM and 100 nM, respectively. The optimized concentrations of the inputs (A2, B2 and C2) for the 3-3 DC system were determined, based on the fluorescence intensities of FAM and Cy5, as 300 nM, 300 nM and 300 nM, respectively (Fig. S7†). Thirdly, in the 4-3 DC logic operation, the concentrations of the DNA switches $P1_{4\text{-}3}$, $P2_{4\text{-}3}$ and $P3_{4\text{-}3}$ were confirmed as 100 nM, 100 nM and 100 nM, respectively. The optimized concentrations of the inputs (A3, B3, C3 and D3) in the operation of the 4-3 DC system were determined, based on the fluorescence intensities of FAM and Cy5, as 350 nM, 300 nM, 300 nM and 350 nM, respectively (Fig. S10†).

2.3. Logic circuit operation

All the DNA sequences were dissolved in deionized water to certain concentrations as stock solutions, and then diluted in Tris-HCl buffer for the hybridization reactions in the logic operations. The DNA-based switches (MBs and G4/NMM) were used as the platform for all the logic operations developed in this investigation, including 2-3 DC, 3-3 DC and 4-3 DC. The required input strands with the corresponding platform were added into the logic system according to the logic operation. The mixture was then annealed under reaction conditions of 90 °C for 10 min and cooled down to room temperature. Subsequently, the optimized concentrations of inputs and certain concentrations of DNA switches were mixed to a final volume of 400 μL, and this was incubated at room temperature for 2 h. The concentration of NMM used in this work was 500 nM for the implementation of digital comparator systems.

2.4. Native polyacrylamide gel electrophoresis (PAGE)

The solutions of DNA strands used in this work were diluted to 2 μM using Tris-HCl buffer solution before the experiments and denatured *via* heating at 90 °C for 10 min. When the solutions had slowly cooled down to room temperature, the desired volumes of the DNA switches in the platform and the corresponding inputs were mixed together and incubated in solution for 30 min. After the preparation of the DNA solution, electrophoresis experiments were carried out in 1× TBE (2 mM EDTA, 17.8 mM Tris, 17.8 mM boric acid, pH 8.0) using 15% native polyacrylamide gel and at a constant voltage of 100 V for about 2 h. Finally, the resulting gels were studied using a UV transilluminator.

3. Results and discussion

The proposed DNA switches were designed as a universal platform for the construction of DNA-based digital comparator systems. In this DC system, 2-3, 3-3 and 4-3 DCs have been suc-

cessfully realized based on the designed platform of DNA switches. The platform consists of two hairpin-shaped MBs (P1 and P3) and a G4/NMM complex (P2) (Fig. 1). P1 was modified with a 6-carboxyfluorescein (FAM, emission max at 517 nm) fluorophore and its corresponding quencher at the two ends of the probe. P3 was modified with Cy5 (emission max at 663 nm) and its corresponding quencher at the two ends. The fluorescence of *N*-methyl mesoporphyrin IX (NMM, emission max at 609 nm) increased obviously when it connected with G4 and formed the resulting G4/NMM complex. The corresponding dim fluorescence of P1 and P3 could be increased when they hybridized with their complementary strands, and the increased P2 NMM fluorescence could decrease when the structure of G4 was destroyed by cytosine-rich (C-rich) inputs (Fig. S1†). The DC logic systems required different numbers of inputs (two inputs, A1 and B1, for 2-3 DC; three inputs, A2, B2, and C2, for 3-3 DC; and four inputs, A3, B3, C3, and D3, for 4-3 DC), with three fluorescence signals as outputs: FAM; NMM; and Cy5.

3.1. The operation of the 2-3 digital comparator

The reaction principle of the DNA switch-based operation for the 2-3 DC is presented in Fig. 2A. In order to explore the optimal experimental conditions, the pH value and buffer concentration used in the experiment were optimized for the successful operation of the DC logic system (Fig. S2†). Furthermore, in the 2-3 DC circuit, different input concentrations were optimized using the DNA switch-based platform (Fig. S3†). The resulting truth table (Fig. S4†) clearly shows that the 2-3 logic system executed the binary comparison operations of A1 > B1 (1 > 0), A1 = B1 (0 = 0 or 1 = 1) and A1 < B1 (0 < 1), with the corresponding output results of $Y1_{2\text{-}3}$, $Y2_{2\text{-}3}$ and $Y3_{2\text{-}3}$ (with high fluorescence intensity from FAM, NMM and Cy5 defined as "1"). For the inputs, the absence of any input was set as "0", however, inputs were set as "1" when they appeared. As shown in Fig. 2A, the DNA switch-based platform contained two MBs ($P1_{2\text{-}3}$ and $P3_{2\text{-}3}$) that were modified at both ends with different fluorescence dyes and their corresponding quenchers, and a G4/NMM complex. Thus, in the initial state of the reaction platform, both $P1_{2\text{-}3}$ (4*-3*-4) and $P3_{2\text{-}3}$ (1-5*-1*) maintained their original hairpin structures and emitted dim fluorescence signals *via* FRET in the absence of the two inputs of A1 (1-2-3-4) and B1 (4*-2-5-1*) (Fig. 2B, curve a and curve i, respectively). Such dim fluorescence outputs from FAM and Cy5 were defined as "0" in the truth table. At the same time, the G4/NMM complex ($P2_{2\text{-}3}$) remained the same and exhibited high fluorescence, defined as "1" in the truth table, representing the output result of A1 = B1 (0 = 0) with the corresponding fluorescence output signal of "010" (Fig. 2B, curve e). In this DC system, the changes in the structures and fluorescence signals of the three DNA switches, $P1_{2\text{-}3}$, $P2_{2\text{-}3}$ and $P3_{2\text{-}3}$, were reversible. When any input was introduced into the platform, it could bind to the toehold region of $P1_{2\text{-}3}$ (3*) or $P3_{2\text{-}3}$ (5*) to initiate a toehold-mediated strand displacement reaction, resulting in the unfolding of $P1_{2\text{-}3}$ or $P3_{2\text{-}3}$ and recovering the fluorescence dyes (FAM or Cy5) *via* FRET. Not only that, the input could also break the structure of G4, resulting in relatively low fluorescence from

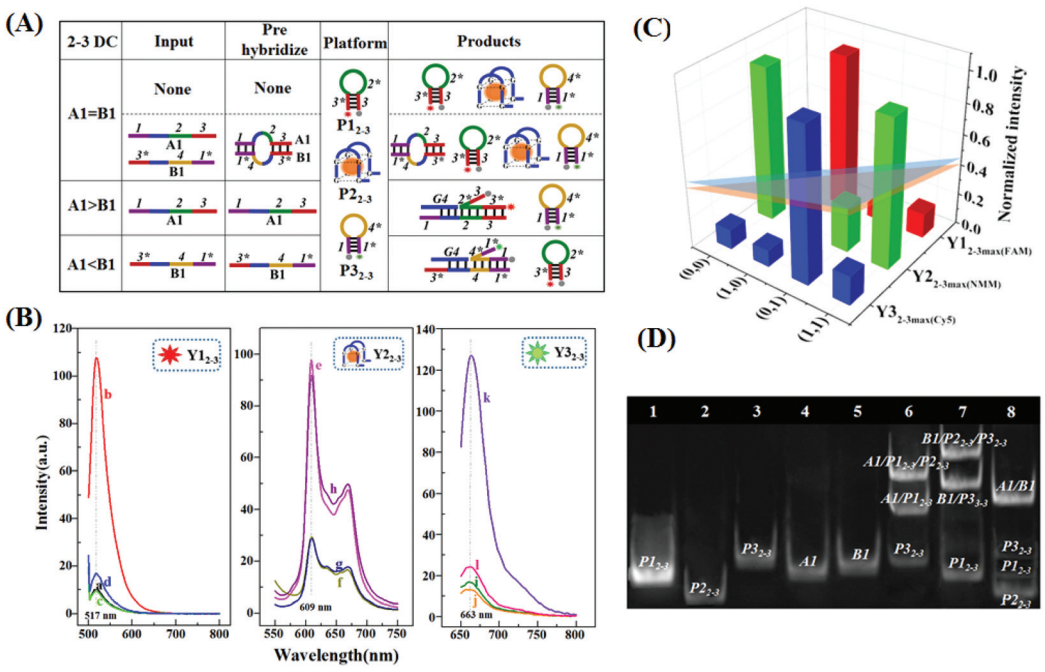

Fig. 2 (A) The operation principle of the 2-3 DC. (B) The intensities of the three output signals (FAM, NMM and Cy5) from the 2-3 DC triggered by the various inputs. (C) A corresponding histogram of the normalized fluorescence responses. (D) PAGE analysis of the 2-3 digital comparator. Different DNA samples were added into lanes 1–8: lane 1: $P1_{2\text{-}3}$; lane 2: $P2_{2\text{-}3}$; lane 3: $P3_{2\text{-}3}$; lane 4: A1; lane 5: B1; lane 6: $P1_{2\text{-}3}$ + $P2_{2\text{-}3}$ + $P3_{2\text{-}3}$ + A1; lane 7: $P1_{2\text{-}3}$ + $P2_{2\text{-}3}$ + $P3_{2\text{-}3}$ + B1; lane 8: $P1_{2\text{-}3}$ + $P2_{2\text{-}3}$ + $P3_{2\text{-}3}$ + A1 + B1.

NMM. Therefore, when A1 was added to the DNA switch-based platform, it could bind to the toehold region (3*) of $P1_{2\text{-}3}$ to initiate a toehold-mediated strand displacement reaction, resulting in the unfolding of $P1_{2\text{-}3}$ and the recovery of the fluorescence of FAM emission at 517 nm (Fig. 2B, curve b). At the same time, A1 could also hybridize with $P2_{2\text{-}3}$, breaking the G4 structure and decreasing the fluorescence of NMM (Fig. 2B, curve f). In this case, the high fluorescence of $P1_{2\text{-}3}$ was defined as "1" and the relatively low fluorescence of NMM was defined as "0" in the truth table, representing the output result of A1 > B1 (1 > 0), with the corresponding fluorescence output expressed as "100". When B1 was input into the platform, it could bind to the toehold region (5*) of $P3_{2\text{-}3}$ and unfold its hairpin structure, leading to the recovery of the fluorescence of Cy5 emission at 663 nm (Fig. 2B, curve k). Such high fluorescence of Cy5 was defined as "1", representing the output result of A1 < B1 (0 < 1). B1 could also hybridize with the platform of $P2_{2\text{-}3}$, breaking the G4 structure and decreasing the fluorescence of NMM (Fig. 2B, curve g), which was defined as "0". The addition of B1 into the platform presented the fluorescence output "001". When A1 and B1 were both introduced into the platform, they reacted with each other and formed a duplex strand of A1 and B1, leaving $P1_{2\text{-}3}$ and $P3_{2\text{-}3}$ alone and resulting in low fluorescence of FAM and Cy5 (Fig. 2B, curve d and curve l), and NMM was also neglected and demonstrated high fluorescence (Fig. 2B, curve h); this generated the result A1 = B1 (1 = 1) and an output fluorescence signal of "010". To implement the function of 2-3 DC, the normalized fluorescence intensities of the three outputs at the peak maxima, $Y1_{2\text{-}3\max(FAM)}$, $Y2_{2\text{-}3\max(NMM)}$ and $Y3_{2\text{-}3\max(Cy5)}$, were plotted as a function of the input combinations (Fig. 2C). Similar to the approach applied in electronic circuits, when the normalized intensity of the fluorescence signal was higher than 0.45, the output was defined as "1". However, when the normalized intensity of the fluorescence signal was lower than 0.4, the output was defined as "0". This definition method was applied to all logic operations in this work.

Native polyacrylamide gel electrophoresis (PAGE) experiments were implemented to demonstrate the hybridization reactions between the inputs and the platform during the 2-3 DC operation (Fig. 2D). All DNA sequences mentioned in this 2-3 logic operation that present in different bands have been determined. From lane 1 to lane 5, the bands presented the DNA switches of $P1_{2\text{-}3}$, $P2_{2\text{-}3}$, and $P3_{2\text{-}3}$, as well as the single DNA input strands of A1 and B1, and all single-stranded DNAs appeared at different positions. When A1 was added into the DNA switch-based platform, two new bands appeared in lane 6. The upper one was proved to be from a duplex of A1/$P1_{2\text{-}3}$/$P2_{2\text{-}3}$ and the lower one was shown to be from a duplex of A1/$P1_{2\text{-}3}$ (see the illustration in Fig. S5†). Upon the addition of B1 into the platform, two new bands appeared, showing the hybridization reactions of B1 with both $P2_{2\text{-}3}$ and $P3_{2\text{-}3}$ in lane 7. However, with the concurrent addition of A1 and B1 into the platform, a new band appeared, which meant that A1 hybridized with B1 as a priority and formed the duplex strand A1/B1, not reacting with the platform at its initial position in lane 8. The PAGE results validated that the DNA reactions of the 2-3 DC logic circuit occurred as expected, consistent with the fluorescence results in Fig. 2B.

3.2. The operation of the 3-3 digital comparator

Further, we explored the versatility of the DNA switch-based platform through designing a 3-3 DC logic circuit, which was an extension of the 2-3 DC and could further contrast a larger range of binary numbers. As shown in the truth table of the 3-3 DC logic circuit (Fig. S6†), a third input, C2 (3*-4-1*-3, also named N for convenience), was introduced into the operation; its function was to be compared with A2 (1-2-3) and B2 (3*-1-2-3), where the inputs of A2 and B2 were converted to a two-bit binary number that was named M for convenience. The resulting truth table (Fig. S6†) clearly shows that the 3-3 DC logic system could execute the binary comparison operations of M = N, M > N and M < N (including the comparisons 00 = 0, 01 = 1, 01 > 0, 10 > 0, 11 > 0, 10 > 1, 11 > 1 and 00 < 1). Before logic operations with the 3-3 DC, the corresponding concentrations of all inputs were optimized based on the DNA switch platform (Fig. S7†). Based on a platform of three DNA switches ($P1_{3\text{-}3}$, $P2_{3\text{-}3}$ and $P3_{3\text{-}3}$), the 3-3 DC was realized (Fig. 3A). Firstly, in the case of M = N, with the fluorescent output of "010" when there was no input into the platform, both $P1_{3\text{-}3}$ and $P3_{3\text{-}3}$ maintained their original hairpin structures and emitted dim fluorescence signals *via* FRET (Fig. 3B, curve a and curve q, respectively). At the same time, the G4/NMM complex ($P2_{3\text{-}3}$) demonstrated high fluorescence, which was defined as "1", representing the logic result A2B2 = C2 (00 = 0) (Fig. 3B, curve i). When B2 and C2 were added into the platform, they reacted with each other as a priority, leaving $P1_{3\text{-}3}$ and $P3_{3\text{-}3}$ unaltered and resulting in low fluorescence from FAM and Cy5 (Fig. 3B, curve g and curve w); the G4/NMM complex retained its original structure and demonstrated high fluorescence (Fig. 3B, curve o), with the result A2B2 = C2 (01 = 1). Secondly, in the case of M > N, with the fluorescent signal output "100", when A2 or B2 was added to the platform, each of them could bind to the toehold region (2*) of $P1_{3\text{-}3}$ and unfold the hairpin structure, recovering the FAM fluorescence (Fig. 3B, curve b and curve c). Not only that, A2 and B2 could also hybridize with the G4 structure of $P2_{3\text{-}3}$, decreasing the NMM fluorescence (Fig. 3B, curve g and curve k). In this case, the high fluorescence of $P1_{3\text{-}3}$ was defined as "1" and the relative low fluorescence of $P2_{3\text{-}3}$ was defined as "0" in the truth table, representing the output result A2B2 > C2 (01 > 0 or 10 > 0). Similar to the reaction mechanism described above, the coexistence of A2 and B2 output the same result, A2B2 > C2 (11 > 0) (Fig. 3B, curve e, curve m and curve u). When the two strands A2 and C2 were input to the platform, A2 was designed to hybridize with not only C2 (1* and 3*) but also $P1_{3\text{-}3}$ and $P2_{3\text{-}3}$, showing high FAM fluorescence, defined as "1", and low NMM fluorescence, defined as "0" (Fig. 3B, curve f and curve n), representing the output result A2B2 > C2 (10 > 1). When A2, B2 and C2 were all introduced into the platform, B2 hybridized with C2 as a priority, inhibiting the chances of C2 to hybridize with $P3_{3\text{-}3}$. At the same time, A2 could hybridize with both $P1_{3\text{-}3}$ and

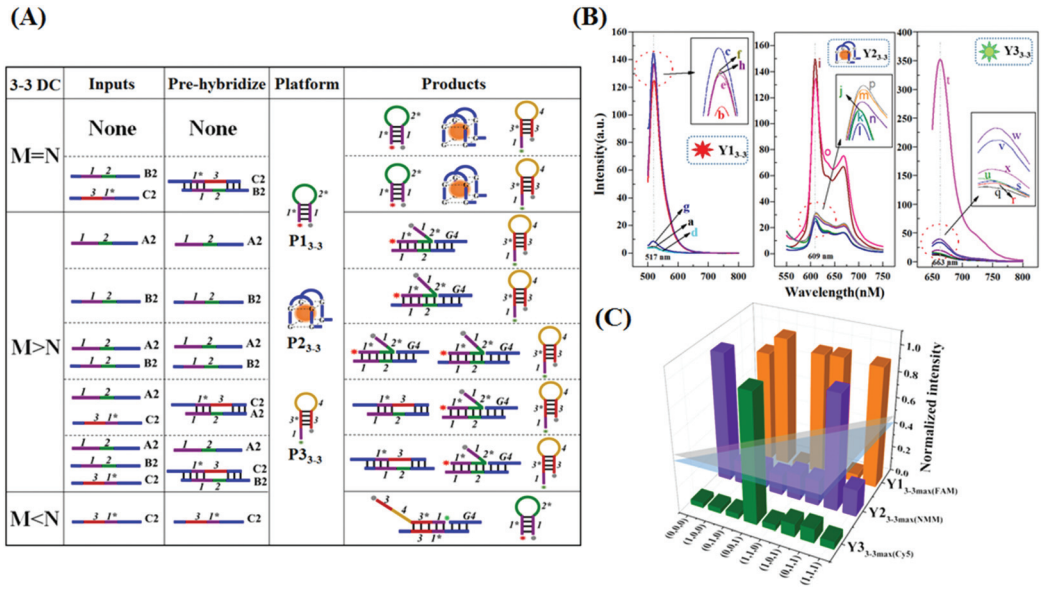

Fig. 3 (A) The operation principle of the 3-3 DC. (B) The intensities of the three output signals (FAM, NMM and Cy5) from the 3-3 DC triggered by the various inputs. (C) A corresponding histogram of the normalized fluorescence responses.

$P2_{3\text{-}3}$, showing high FAM fluorescence and low NMM fluorescence, with the output A2B2 > C2 (11 > 1) (Fig. 3B, curve h and curve p). Thirdly, in the case of M < N, with the fluorescent output signal "001" when only C2 was input into the platform, C2 could hybridize with $P2_{3\text{-}3}$ and bind to the toehold region (5) of $P3_{3\text{-}3}$, resulting in high Cy5 fluorescence and relatively low NMM fluorescence (Fig. 3B, curve t and curve l), representing the output result A2B2 < C2 (00 < 1).

To utilize the functionality of the 3-3 DC, the normalized fluorescence intensities of the three outputs at the peak maxima, $Y1_{3\text{-}3max(FAM)}$, $Y2_{3\text{-}3max(NMM)}$ and $Y3_{3\text{-}3max(Cy5)}$, were plotted as a function of the input combinations (Fig. 3C). The threshold value for the output was defined as "1" when the normalized intensity of the fluorescence signal was higher than 0.45. However, when the normalized intensity of the fluorescence signal was less than 0.4, the threshold value for the output could be defined as "0". PAGE experiments were performed to further identify the hybridization between the inputs and the platform during the 3-3 DC operations (Fig. S8†). These experimental results have fully proven the feasibility of our strategy for the operation of the 3-3 DC logic circuit, and were consistent with the fluorescence results shown Fig. 3B.

3.3. The operation of the 4-3 digital comparator

The basic principle of DNA-based logic operation design is to engineer operation information into the DNA sequences through programming complementarity between the inputs and the reaction platform. In order to continue to expand the range of DNA-based DC operation systems, more DNA input signals were programmed and designed. In this work, a 4-3 DC was conceptually implemented, with a fourth input (D3) added into the platform (Fig. 4A). The corresponding truth table (Fig. S9†) shows that the 4-3 DC logic circuit executed the binary comparison operations of X > Y, X = Y and X < Y, where X represents the combination of the A3 (1-1*-2-3-1-4) and B3 (3*-2-1*-1) inputs as a two-bit binary number and Y represents the combination of the C3 (3*-2*-1-1*-4-2*-3) and D3 (4*-1*-1-2*-3*) inputs as a two-bit binary number for convenience. Before logic operations with the 4-3 DC, the corresponding input concentrations were optimized with the DNA switch-based platform (Fig. S10†). The operation of the 4-3 DC was carried out based on a platform that consisted of three DNA switches ($P1_{4\text{-}3}$, $P2_{4\text{-}3}$ and $P3_{4\text{-}3}$) (Fig. 4A). Firstly, in the case of X = Y, with the corresponding fluorescent signal output of "010" when no inputs were introduced into the platform, both $P1_{4\text{-}3}$ and $P3_{4\text{-}3}$ maintained their hairpin structures and emitted dim fluorescence signals *via* FRET (Fig. 4B, curve a1 and curve i1, respectively). Also, the G4/NMM complex ($P2_{4\text{-}3}$) remained the same and demonstrated high fluorescence, defined as "1", representing the output result A3B3 = C3D3 (00 = 00) (Fig. 4B, curve e1). When A3 and C3 coexisted, they preferred to hybridize with each other, while they did not hybridize with the DNA-based switches; this resulted in low FAM and Cy5 fluorescence, defined as "0" (Fig. 4B, curve b1 and curve j1), and high NMM fluorescence, defined as "1" (Fig. 4B, curve f1). Such performance showed the logic operation result A3B3 = C3D3 (10 = 10). When B3 and D3 coexisted, they also preferred to hybridize with each other and showed low FAM and Cy5 fluorescence, defined as "0" (Fig. 4B, curve c1 and curve k1), and high NMM fluorescence, defined as "1" (Fig. 4B, curve g1), representing the logic result A3B3 = C3D3 (01 = 01). Similar to the reaction mechanism described above, when all the inputs, A3, B3, C3 and D3, were input into the platform, they had a preference for hybridization with each other; this also resulted in low FAM and Cy5 fluorescence, defined as "0"

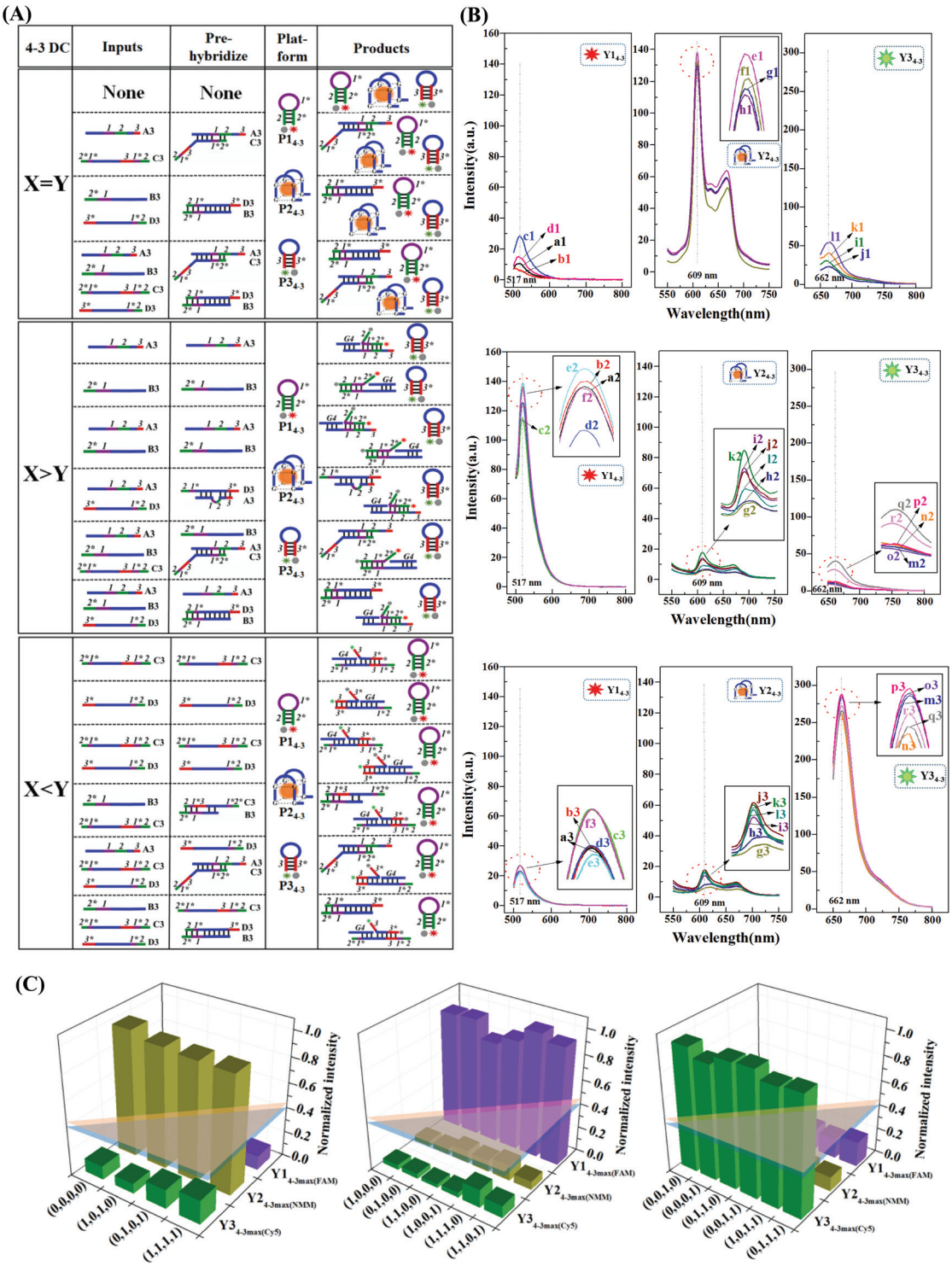

Fig. 4 (A) The operation principle of the 4-3 DC. (B) The intensities of the three output signals (FAM, NMM and Cy5) from the 4-3 DC triggered by the various inputs. (C) A corresponding histogram of the normalized fluorescence responses.

(Fig. 4B, curve d1 and curve l1), and high NMM fluorescence, defined as "1" (Fig. 4B, curve h1), representing the logic result A3B3 = C3D3 (11 = 11). Secondly, in the case of X > Y with the corresponding fluorescence output signal of "100", when A3 or B3 was added to the platform, each of them could break the G4 structure of $P2_{4\text{-}3}$ and bind to the toehold region (2*) of $P1_{4\text{-}3}$, resulting in high FAM fluorescence (Fig. 4B, curve a2 and curve b2) and relatively low NMM fluorescence (Fig. 4B, curve g2 and curve h2). In this case, the high fluorescence of $P1_{4\text{-}3}$ was defined as "1" and the relative low fluorescence of

$P2_{4\text{-}3}$ was defined as "0", representing the output result A3B3 > C3D3 (10 > 00 or 01 > 00). Similar to the reaction mechanism described above, the coexistence of A3 and B3 generated the same result: A3B3 > C3D3 (11 > 00) (Fig. 4B, curve c2, curve i2 and curve o2). With the addition of A3 and D3 to the platform, A3 was designed to hybridize with not only D3 (1, 1* and 4*) but also $P1_{4\text{-}3}$ (2*) and $P2_{4\text{-}3}$, showing high FAM fluorescence, defined as "1", and low NMM fluorescence, defined as "0" (Fig. 4B, curve d2 and curve j2), representing the output result A3B3 > C3D3 (10 > 01). When A3, B3 and C3 were introduced into the platform, A3 hybridized with C3 as a priority, and B3 could hybridize with $P2_{4\text{-}3}$ and bind to the toehold region of (2*) of $P1_{4\text{-}3}$, resulting in high FAM fluorescence and low NMM fluorescence with the output A3B3 > C3D3 (11 > 01) (Fig. 4B, curve e2 and curve k2). When strands of A3, B3 and D3 were input into the platform, B3 preferentially reacted with D3, and A3 could hybridize with $P2_{4\text{-}3}$ and bind to the toehold region of (2*) of $P1_{4\text{-}3}$; this resulted in high FAM fluorescence and low NMM fluorescence, with the output A3B3 > C3D3 (11 > 10) (Fig. 4B, curve f2 and curve l2). Thirdly, in the case of X < Y with the corresponding fluorescence output signal of "001", when C3 or D3 was added to the platform, each of them could break the G4 structure of $P2_{4\text{-}3}$ and bind to the toehold region (1) of $P3_{4\text{-}3}$, resulting in high Cy5 fluorescence (Fig. 4B, curve m3 and curve n3) and relatively low NMM fluorescence (Fig. 4B, curve g3 and curve h3). Under these conditions, the high $P3_{4\text{-}3}$ fluorescence was defined as "1" and the relatively low $P2_{4\text{-}3}$ fluorescence was defined as "0", representing the output result A3B3 < C3D3 (00 < 10 or 00 < 01). Similar to the reaction mechanism described above, the coexistence of C3 and D3 generated the same result: A3B3 < C3D3 (00 < 11) (Fig. 4B, curve c3, curve i3 and curve o3). With the addition of B3 and C3 to the platform, C3 was designed to hybridize with not only B3 but also $P2_{4\text{-}3}$ and $P3_{4\text{-}3}$; this resulted in high Cy5 fluorescence, defined as "1", and low NMM fluorescence, defined as "0" (Fig. 4B, curve p3 and curve j3), representing the output result A3B3 < C3D3 (01 < 10). When A3, C3 and D3 were introduced into the platform, C3 would preferentially hybridize with A3, and D3 could hybridize with $P2_{4\text{-}3}$ and bind to the toehold region (1) of $P3_{4\text{-}3}$, resulting in high Cy5 fluorescence and low NMM fluorescence, with the output A3B3 < C3D3 (10 < 11) (Fig. 4B, curve q3 and curve k3). Upon the addition of B3, C3 and D3 to the platform, D3 preferred to react with B3, and C3 could hybridize with $P2_{4\text{-}3}$ and $P3_{4\text{-}3}$, resulting in high Cy5 fluorescence and low NMM fluorescence, with the output A3B3 < C3D3 (01 < 11) (Fig. 4B, curve r3 and curve l3). The normalized fluorescence intensities of the three outputs at the peak maxima, $Y1_{4\text{-}3max(FAM)}$, $Y2_{4\text{-}3max(NMM)}$ and $Y3_{4\text{-}3max(Cy5)}$, were plotted for the 4-3 DC as a function of the input combinations (Fig. 4C). The output threshold value was defined as "1" when the normalized fluorescence intensity was higher than 0.45. On the contrary, the output threshold value could be defined as "0" when the normalized fluorescence intensity was lower than 0.4. The DNA interactions were validated through PAGE experiments (Fig. S11†).

3.4. Operations to further verify the DNA selectivity

Logic operations have introduced a new concept into analytical chemical and biomedicine for multi-target detection.[44,45] To demonstrate the multifunctionality of the DNA switch-based platform, this DNA logic system was further explored in an intelligent biosensor to implement selective detection for the first time. Acquired immune deficiency syndrome (AIDS) is a serious infectious disease induced by human immunodeficiency virus (HIV), which can attack and destroy the host immune system, leading to death due to a lack of resistance to many diseases.[46] In addition, it has been reported that about one third of HIV patients are co-infected with hepatitis C virus (HCV), since HCV and HIV share a common transmission path.[47] Thus, it is critical to detect HIV and HCV at an early stage to improve the accuracy of diagnosis and the probability of a cure. In this work, synthetic oligonucleotide sequences from HIV and HCV gene segments were used as the model targets to validate logic-controlled selective detection *via* 2-3 DC logic operations. To realize 2-3 DC-based gene selective detection, two hairpin-shaped MBs (P01 and P03) and a G4/NMM complex (P02) were used as the platform (Fig. 5A). To further realize one-base mismatched sensitivity, different input concentrations were optimized using the DNA switch-based platform (Fig. S12†). As shown in Fig. 5(A), the input sequence A0 (1-2-3-4-5-1*) was designed to contain an oligonucleotide sequence from the HIV gene (4-5). When A0 (containing the HIV gene sequence) was added to the system, A0 could hybridize with both P01 and P02. At this time, the intensity of FAM fluorescence increased and the intensity of NMM fluorescence decreased. B0 (1-4*-3*-2*-1*) was designed to contain a sequence from the HCV gene (3*-2*). When B0 (containing the HCV gene sequence) was added to the system, B0 could hybridize with both P03 and P02. At this time, the intensity of Cy5 fluorescence increased and the intensity of NMM fluorescence decreased. Based on the above-described input sequence encoding and the corresponding changes in dual fluorescence output, the HIV and HCV genes were successfully detected based on the 2-3 logic system. In the initial state of the 2-3 DC logic system, the platform emitted dim FAM and Cy5 fluorescence signals and high NMM fluorescence when no target genes were introduced, expressing the binary comparison operation A0 = B0 and the output signal "010" (Fig. 5B, curve e). In the presence of A0, which contains the HIV gene sequence, A0 could bind to the toehold region of P01 (4*) and destroy the G4 structure of P02, resulting in high FAM fluorescence (Fig. 5B, curve b) and relatively low NMM fluorescence (Fig. 5B, curve f). Therefore, an input of only A0 expressed the comparison A0 > B0 (10) and the output result "100" from the logic operation. In the presence of B0, the HCV gene, B0 could bind to the toehold region of P03 (3) and destroy the G4 structure of P02, which significantly enhanced the Cy5 fluorescence (Fig. 5B, curve k) and inhibited the NMM fluorescence (Fig. 5B, curve g). Therefore, the B0 input expressed the comparison A0 < B0 (01) and the output result "001". When A0 and B0 coexisted,

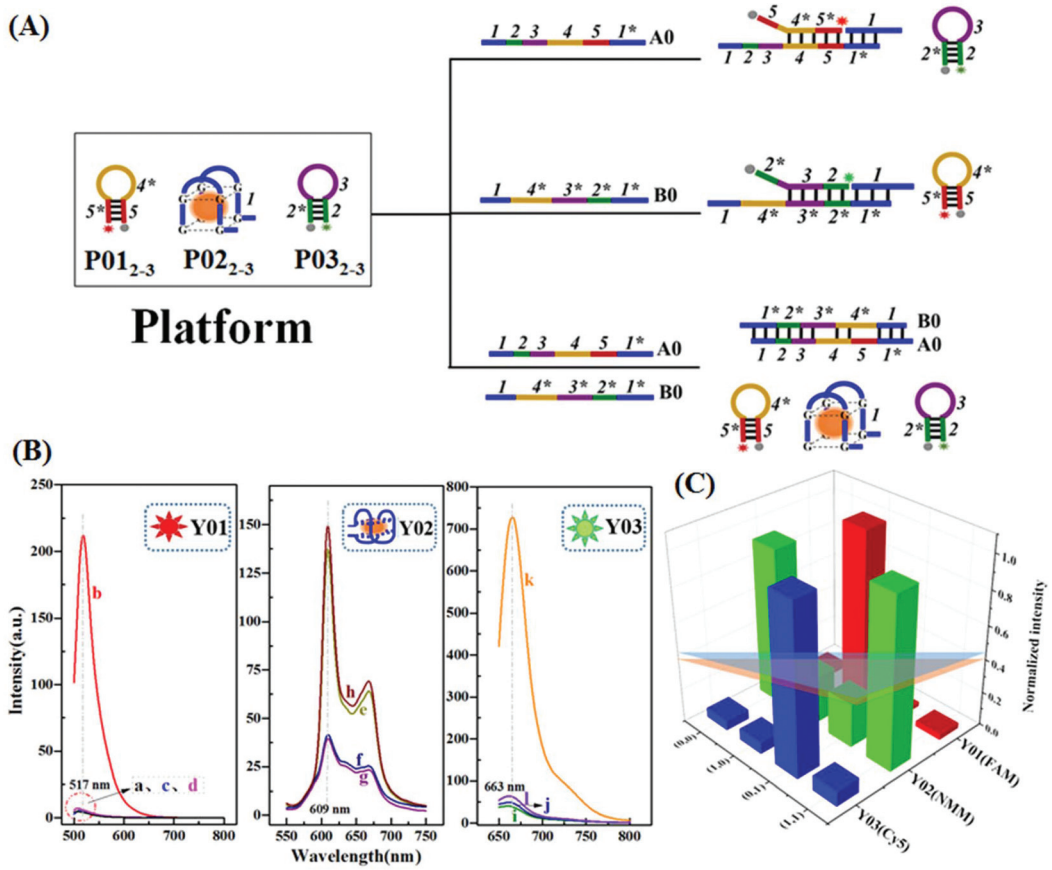

Fig. 5 (A) The reaction principle of the 2-3 DC controlled biosensor for the sensitive detection of HIV and HCV. (B) The intensities of the three output signals (FAM, NMM and Cy5) from the 2-3 DC controlled biosensor triggered by the various inputs. (C) A corresponding histogram of the normalized fluorescence responses.

they preferred to hybridize with each other, which maintained high NMM fluorescence (Fig. 5B, curve h) and had no influence on FAM and Cy5 fluorescence (Fig. 5B, curve d and curve l). When A0 and B0 were concurrently added into the platform, the comparison A0 = B0 (11) was implemented and the corresponding output result was expressed as "010". The results demonstrated that the 2-3 DC could report a high FAM output signal of "1" in the presence of the HIV gene and a high Cy5 output signal of "1" in the presence of the HCV gene. Through plotting the normalized fluorescence of FAM, NMM and Cy5 against various input combinations (Fig. 5C), the 2-3 DC logic operation could transfer the state of the HIV

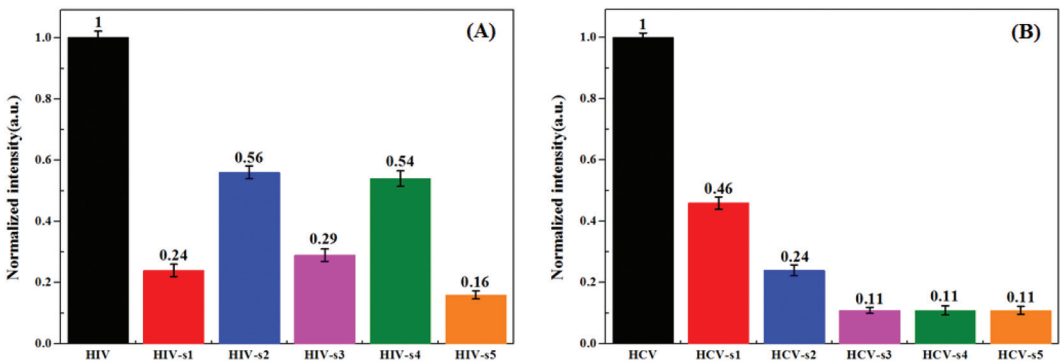

Fig. 6 (A) An illustration of the selectivity of the proposed strategy for DNA detection based on output signals (FAM) for the target HIV DNA against single-base (HIV-s1), two-base (HIV-s2 and HIV-s3), and three-base (HIV-s4 and HIV-s5) mismatched DNA. (B) An investigation of the selectivity of the proposed strategy for DNA detection based on output signals (Cy5) for the target HCV DNA against single-base (HCV-s1), two-base (HCV-s2 and HCV-s3), and three-base (HCV-s4 and HCV-s5) mismatched DNA.

gene into the specific output channel Y01 and could transmit the state of the HCV gene into the specific output channel Y03 based on the platform of DNA switches.

Selectivity is significant for DNA biosensors, and our developed DC logic system has been further proved to present excellent selectivity for the detection of HIV and HCV. As shown in Fig. 6, the system exhibited different fluorescence intensities in the presence of the target genes and different corresponding base mismatched DNA samples. In Fig. 6A, the fluorescence signals caused by one-base mismatched DNA (HIV-s1), two-base mismatched DNA (HIV-s2 and HIV-s3), and three-base mismatched DNA (HIV-s4 and HIV-s5) were 24%, 56%, 29%, 54%, and 16% of that caused by the target DNA, HIV, respectively. In Fig. 6B, the fluorescence signals generated by one-base mismatched DNA (HCV-s1), two-base mismatched DNA (HCV-s2 and HCV-s3), and three-base mismatched DNA (HCV-s4 and HCV-s5) were 46%, 24%, 11%, 11%, an 11% of that caused by the target DNA of HCV. As expected, the 2-3 DC logic-based system showed obvious responses to HIV and HCV through corresponding fluorescence signals, while negligible responses were observed for all other mismatched DNA strands, indicating that the proposed target-driven DNA switch-based platform could distinguish single-base mutations and exhibit excellent selectivity for both HIV and HCV detection. PAGE experiments were performed, and they fully proved the occurrence of the reactions between the platform and inputs (Fig. S13†).

4. Conclusions

In conclusion, this work has successfully demonstrated the design of a novel strategy for the wireless operation of DNA-based digital comparator systems based on a simple and universal DNA switch-based platform. To the best of our knowledge, this is the first time that a library of digital comparators (2-3 DC, 3-3 DC and 4-3 DC) with three outputs has been constructed using a multifunctional DNA switch-based platform to implement operations that compare whether two or more input binary codes are equal. Through the step-by-step realization of DC logic operations with different input signals, such DC logic systems lay the foundation for the development of DC systems that show functionality involving large-scale input signals based on powerful DNA hybridization, as well as solving the problems of design complexity and manufacturing cost related to the integrated circuits used in traditional computing. In this study, apart from a futuristic vision for DNA-based digital comparator systems, we also introduced the selective detection of HIV and HCV genes at the single-base mismatch level under 2-3 DC logic control. The proposed strategy was expanded to logic operation design applications, and exhibited high performance not only for molecular computing applications but also for DNA selective analysis, providing a promising method for the integration of complex DNA devices and selective detection.

Conflicts of interest

The authors declare no conflicts of interest.

Acknowledgements

This work was supported by the National Natural Science Foundation of China (NSFC, 91750205, 21404015, 61774155, 61705227), the National Key Research and Development Program of China (2017YFB1104700, 2018YFB1107202), the K. C. Wong Education Foundation (GJTD-2018-08), and the Jilin Science and Technology Department Project (20180414019GH).

References

1 Y. V. Gerasimova and D. M. Kolpashchikov, *Angew. Chem., Int. Ed.*, 2016, **55**, 10244–10247.
2 A. Malvino and J. Brown, *Digital Computer Electronics*, Glencoe, Lake Forest, 3rd edn, 1993.
3 K. S. Park, M. W. Seo, C. Jung, J. Y. Lee and H. G. Park, *Small*, 2012, **8**, 2203–2212.
4 F. Wang, C. Lu and I. Willner, *Chem. Rev.*, 2014, **114**, 2881–2941.
5 M. Stojanovic, D. Stefanovic and S. Rudchenko, *Acc. Chem. Res.*, 2014, **47**, 1845–1852.
6 F. Pu, J. Ren and X. Qu, *Adv. Mater.*, 2014, **26**, 5742–5757.
7 H. Li, W. Hong, S. Dong, Y. Liu and E. Wang, *ACS Nano*, 2014, **8**, 2796–2803.
8 L. M. Adleman, *Science*, 1994, **266**, 1021–1024.
9 L. Qian and E. Winfree, *Science*, 2011, **332**, 1196–1201.
10 D. Y. Tam, Z. W. Dai, M. S. Chan, L. S. Liu, M. C. Cheung, F. Bolze, C. Tin and P. K. Lo, *Angew. Chem., Int. Ed.*, 2016, **55**, 164–168.
11 C. Y. Zhou, K. Wang, D. Q. Fan, C. T. Wu, D. L. Liu, Y. Q. Liu and E. K. Wang, *Chem. Commun.*, 2015, **51**, 10284.
12 C. Y. Zhou, C. T. Wu, Y. Q. Liu and E. K. Wang, *RSC Adv.*, 2016, **6**, 106641.
13 J. Chen, S. Zhou and J. Wen, *Angew. Chem., Int. Ed.*, 2015, **54**, 446–450.
14 J. Elbaz, F. Wang, F. Remacle and I. Willner, *Nano Lett.*, 2012, **12**, 6049–6054.
15 C. Y. Zhou, D. L. Liu, C. T. Wu, Y. Q. Liu and E. K. Wang, *Nanoscale*, 2016, **8**, 17524.
16 C. Y. Zhou, D. L. Liu, C. T. Wu, S. J. Dong and E. K. Wang, *ACS Appl. Mater. Interfaces*, 2016, **8**, 30287.
17 C. Y. Zhou, H. M. Geng and C. L. Guo, *Acta Biomater.*, 2018, **80**, 58.
18 S. Bi, M. Chen, X. Jia, Y. Dong and Z. Wang, *Angew. Chem., Int. Ed.*, 2015, **54**, 8144–8148.
19 W. Engelen, L. H. Meijer, B. Somers, T. F. de Greef and M. Merkx, *Nat. Commun.*, 2017, **8**, 14473.
20 J. Zhu, L. Zhang, T. Li, S. Dong and E. Wang, *Adv. Mater.*, 2013, **25**, 2440–2444.

21 N. V. DelRosso, S. Hews, L. Spector and N. D. Derr, *Angew. Chem., Int. Ed.*, 2017, **56**, 4443–4446.
22 C. Y. Zhou, D. L. Liu and S. J. Dong, *ACS Appl. Mater. Interfaces*, 2016, **8**, 20849.
23 K. He, Y. Li, B. Xiang, P. Zhao, Y. Hu, Y. Huang, W. Li, Z. Nie and S. Yao, *Chem. Sci.*, 2015, **6**, 3556–3564.
24 T. Li, E. K. Wang and S. J. Dong, *J. Am. Chem. Soc.*, 2009, **131**, 15082–15083.
25 L. Ma and A. P. Diao, *Chem. Commun.*, 2015, **51**, 10233–10235.
26 S. Bi, B. Ji, Z. Zhang and J. Zhu, *Chem. Sci.*, 2013, **4**, 1858–1863.
27 G. Seelig, D. Soloveichik, D. Y. Zhang and E. Winfree, *Science*, 2006, **314**, 1585–1588.
28 R. Peng, X. Zheng, Y. Lyu, L. Xu, X. Zhang, G. Ke, Q. Liu, C. You, S. Huan and W. Tan, *J. Am. Chem. Soc.*, 2018, **140**, 9793–9796.
29 J. Yang, R. Wu, Y. Li, Z. Wang, L. Pan, Q. Zhang, Z. Lu and C. Zhang, *Nucleic Acids Res.*, 2018, **46**, 8532–8541.
30 N. C. Seeman, *Annu. Rev. Biochem.*, 2010, **79**, 65–87.
31 Y. Tang, B. Ge, D. Sen and H. Yu, *Chem. Soc. Rev.*, 2014, **43**, 518–529.
32 C. Y. Zhou, Z. Yu, W. L. Yu, H. W. Liu, H. Zhang and C. L. Guo, *Microchim. Acta*, 2019, **186**, 4.
33 D. Q. Fan, J. B. Zhu, Q. F. Zhai, E. K. Wang and S. J. Dong, *Chem. Commun.*, 2016, **52**, 3766–3769.
34 D. Q. Fan, E. K. Wang and S. J. Dong, *Mater. Horiz.*, 2017, **4**, 924–931.
35 H. Pei, L. Liang, G. B. Yao, J. Li, Q. Huang and C. H. Fan, *Angew. Chem., Int. Ed.*, 2012, **51**, 9020–9024.
36 E. M. Willner, Y. Kamada, Y. Suzuki, T. Emura, K. Hidaka, H. Dietz, H. Sugiyama and M. Endo, *Angew. Chem., Int. Ed.*, 2017, **56**, 15324–15328.
37 S. Tyagi and F. R. Kramer, *Nat. Biotechnol.*, 1996, **14**(3), 303–308.
38 D. Sen and W. Gilbert, *Nature*, 1988, **334**, 364–366.
39 J. R. Rubens, G. Selvaggio and T. K. Lu, *Nat. Commun.*, 2016, **7**, 11658.
40 J. Hemphill and A. Deiters, *J. Am. Chem. Soc.*, 2013, **135**, 10512–10518.
41 Z. Xie, L. Wroblewska, L. Prochazka, R. Weiss and Y. Benenson, *Science*, 2011, **333**, 1307–1311.
42 W. C. Liao, Y. S. Sohn, M. Riutin, A. Cecconello, W. J. Parak, R. Nechushtai and I. Willner, *Adv. Funct. Mater.*, 2016, **26**, 4262–4273.
43 K. Wang, D. Fan, Y. Liu and S. Dong, *Biosens. Bioelectron.*, 2017, **87**, 116–121.
44 D. Han, H. Kang, T. Zhang, C. Wu, C. Zhou, M. You, Z. Chen, X. Zhang and W. Tan, *Chem. – Eur. J.*, 2014, **20**, 5866–5873.
45 Y. H. Lai, S. C. Sun and M. C. Chuang, *Biosens. Bioelectron.*, 2014, **4**, 273–300.
46 X. Lin, Y. Liu, Z. Tao, J. Gao, J. Deng, J. Yin and S. Wang, *Biosens. Bioelectron.*, 2017, **94**, 471–477.
47 M. D. Hernandez and K. E. Sherman, *Curr. Opin. HIV AIDS*, 2011, **6**, 478–482.

